ISSN (Print) 1226-1750
ISSN (Online) 2233-6656
Journal of Magnetics 23(3), 480-485 (2018) https://doi.org/10.4283/JMAG.2018.23.3.480

Magnetically Axial-coupled Detachable Propeller-based Portable Electromagnetic Energy-harvesting Device Using Air and Water Streams

Ja Sung Lee and Sung Hoon Kim*

Department of Electronics Convergence Engineering, Wonkwang University, 460 Iksandae-ro, Iksan, Jeonbuk 54538, Republic of Korea

(Received 22 May 2018, Received in final form 18 September 2018, Accepted 20 September 2018)

Energy harvesting has become a highly important technology due to the development of portable electronic devices. In this study, we developed a rotary-type portable electromagnetic energy-harvesting device for charging portable electronic devices from wind and water stream. The advantage of the developed device is that it does not use a mechanical shaft because it uses the magnetic axial coupling (magnetic force) between the turbine and the device. In other words, the turbine can be easily replaced depending on the energy source. Furthermore, the device can produce the electrical power of mW class at a low rotating speed. The device consists of four inducing magnets, 16 pick-up coils, and a coupling magnet for combination between the device and the turbine. The device generated 35.15 V_{rms} at 300 rpm (5 Hz), and the maximum conversion efficiency reached up to 13.52 % at 240 rpm. We are aiming for energy conversion at a low rotational speed under 400 rpm and the device achieved mW class conversion: 360 rpm produced approximately 14 mW. To verify the proposed methods, we conduced various experimental analyses.

Keywords : electromagnetic energy-harvesting, rotary-type generator, magnetic axial-coupling, detachable propeller

1. Introduction

Energy harvesting devices have been widely developed and extensively reported [1-5]. In general, energy-harvesting devices utilize piezoelectric, electrostatic, and electromagnetic (EM) methods. Piezoelectric generators convert vibration into a voltage output, but they generate relatively high voltage (to a maximum of hundreds of V) and low electrical current [6-8], and electrostatic generators provide a relatively high output voltage [9, 10]. Meanwhile, EM generators produce comparatively high output current levels at low output voltages [11, 12]. The output voltage and current depend on the magnet properties, the moving velocity, and the number of turns in the coil. Energy-harvesting devices can be used for biomedical applications or charging portable electronic devices, such as smart phones, notebook computers, and lanterns [13-16]. In addition, the devices can be applied as a permanent power source for wireless water meter readings based on wireless sensor networks. For these functions, energy-harvesting devices must generate minimum of scores of mW. In this study, we developed an EM energy-harvesting device, a portable rotary-type generator, using fluid and air streams. The harvesting device utilizes a permanent axial flux magnet structure, and it consists of four permanent magnets, 16 pick-up coils, and a single axial-coupling magnet for easy installation of the turbine. Because the axial-coupling magnet allows for an easily detachable turbine according to changes in the environment, the proposed device can use tap water and gas flows as energy sources, as shown in Fig. 1. In general, most generators are made in all-in-one types with turbine. Therefore, it is limited to one application. However, the proposed device is independent of the generator and the turbine. The two parts are magnetically coupled without a mechanical shaft. The rotation of the generator is synchronized with the rotation of the turbine by magnetic coupling (magnetic torque). Thus, the proposed structure can be used in a number of applications. In particular, this study aims to generate mW class at a low rotational speed. The developed device was characterized in the range of up to 300 rpm. Under the condition, the device generated 35.15 Vrms and 12 mW at a rotating speed of 300 rpm and a 100 kΩ load. The maximum efficiency is

*Corresponding author: Tel: +82-63-850-6739
Fax: +82-63-850-6739, e-mail: kshoon@wku.ac.kr

Fig. 1. (Color online) Concept of energy harvesting.

13.52 % at 240 rpm with a 100 kΩ load. Through various experimental analyses, we conducted a performance evaluation of the proposed device.

2. Mechanism and Fabrication of the Energy-harvesting Device

2.1. Configuration of the proposed energy-harvesting device

An EM energy-harvesting device utilizes EM induction method for large- to small-scale power generation as a rotating or linear device. The proposed device adopts a rotating mechanism and the proposed magnetic axial coupling provides the coupling between the generator and propeller without mechanical shaft. Therefore, we can adjust the starting torque of the generator by adjusting the coupling distance between two coupling magnets at the generator and propeller. We were able to predict the proper design and distribution of magnetic flux density through simulation, as shown in Fig. 2(a). In this simulation, we investigated distribution of magnetic flux density according to changes in the rotating angles of the magnets on the disc. When the pick-up coil and magnet match, approximately 0.1 T will be induced the single

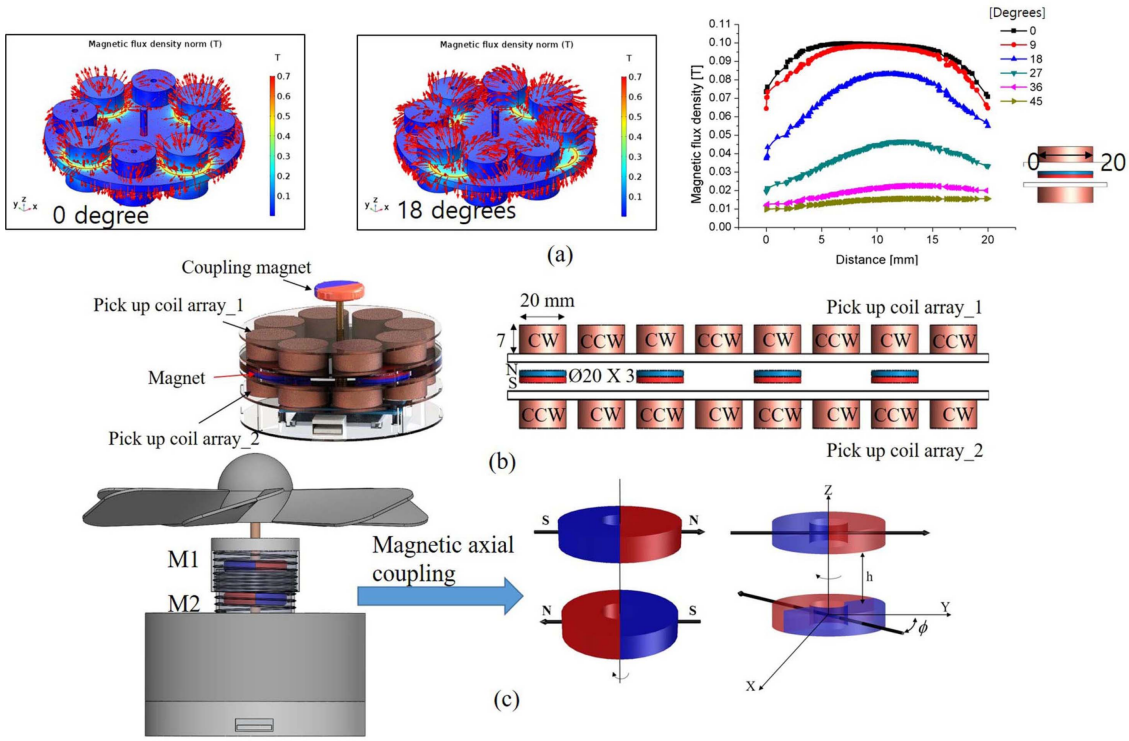

Fig. 2. (Color online) (a) Magnetic simulation results to observe the distribution of magnetic field density in the proposed design. (b) The proposed electromagnetic energy harvesting device with configuration of pick-up coils and magnets. (c) The mechanism of the detachable propeller using magnetic axial coupling and synchronous axial coupling between two magnets with a rotating mechanism through magnetic axial coupling; h denotes the distance between the two magnets, and Φ is the angular displacement.

coil (diameter of 20 mm).

Figure 2(b) shows the configuration of the generator. The device consists of 16 pick-up coils (two arrays) and 4 magnets in total for EM induction. The four magnets are arranged at 90-degree intervals in the same pole direction. The diameter and thickness of the magnet are 20 mm and 3 mm, respectively, and surface flux density is approximately 350 mT. The device's coupling magnet rotates the disk through magnetic axial coupling with the propeller magnet. The magnetization of the coupling magnet is in the diametrical direction. When the propeller rotates, the coupling magnet rotates synchronously with the propeller magnet. The number of turns, diameter, and height of a single pick-up coil is 13000, 20 mm, and 7 mm, respectively. Because of the magnet's pole direction, the winding direction of the pick-up coils intersects clockwise (CW) and counterclockwise (CCW), as shown in Fig. 2 (b). The distance between the magnet and the pick-up coil is 3 mm. When the disk with the magnet is rotated, the magnetic flux density of the four magnets is induced in the pick-up coil to generate electric power. The voltage generated from rotation of a magnet can be expressed as follows:

$$V = N\frac{d\Phi(t)}{dt} = \Omega N\hat{\Phi}\cos(\Omega t) \tag{1}$$

$$V_{\max} = N \cdot n_p \cdot \Phi \cdot \left(rpm \cdot \frac{2\pi}{60}\right) \tag{2}$$

where N is the number of turns; Φ is the total flux linkage of the N-turn coil; Ω is the mechanical angular speed of the rotor; and n_p is the number of poles.

Figure 2(c) shows the method of incorporating a detachable propeller with the device using magnetic axial coupling. The configuration of the two permanent magnets between the propeller and the device cause the magnetic axial coupling. The coupling force is dependent on the distance between the two magnets. In addition, the changes in the coupling force causes the variations in the driving torque with the driving range. The coupling force of the developed device is controlled by the screw mechanism (bolt and nut) of the device housing, as shown in Fig. 2(c). The magnetization directions of M1 and M2 magnets are in the diametrical direction and their axial coupling generate magnetic torque. When the M1 rotates, M2 is synchronized by magnetic torque between M1 and M2. The turbine section and the generator are secured using bolt and nut mechanisms. The magnetic axial coupling force and torque between M1 and M2 magnets are determined by adjusting the position (distance) of the thread.

For magnetic axial coupling, the magnetization of the two magnets is in the diametrical direction. Under the condition, magnetic force and torque from an opposing pole surface can be expressed as follows [17]:

$$F_{z,surf}(h,\phi_s) = \frac{\mu_0 M_s^2}{4\pi}\left\{\pi\frac{(R_2^2-R_1^2)}{n_p N_r N_\phi}\right\}\sum_{i=1}^{N_r}\sum_{j=1}^{N_\phi} \times \sum_{i'=1}^{N_r}\sum_{j'=1}^{N_\phi}\frac{d}{[r_i^2+r_{i'}^2-2r_i r_{i''}(\phi_j-\phi_{j'})+h^2]^{3/2}} \tag{3}$$

$$T_{z,surf}(h,\phi_s) = \frac{\mu_0 M_s^2}{4\pi}\left\{\pi\frac{(R_2^2-R_1^2)}{n_p N_r N_\phi}\right\}\sum_{i=1}^{N_r}\sum_{j=1}^{N_\phi} \times \sum_{i'=1}^{N_r}\sum_{j'=1}^{N_\phi}\frac{r_i r_{i'}\sin(\phi_j-\phi_{j'})}{[r_i^2+r_{i'}^2-2r_i r_{i'}\cos(\phi_j-\phi_{j'})+h^2]^{3/2}} \tag{4}$$

where N_r and N_φ denote the number of mesh variables, and R_1 and R_2 are the inner and outer radii, respectively. Finally, (r_i, φ_j) is the midpoint of the element ΔS. The summing point charges on the surface mesh became a surface area ($\Delta S = \pi(R_2^2 - R_1^2)/N_{pole}N_r N_\phi$), h and μ_0 is the distance between the two magnets and the permeability of free space, respectively.

2.2. Fabrication of the energy-harvesting device

Figure 3(a) shows the fabricated harvesting device with the two propellers for air stream (center) and water flow

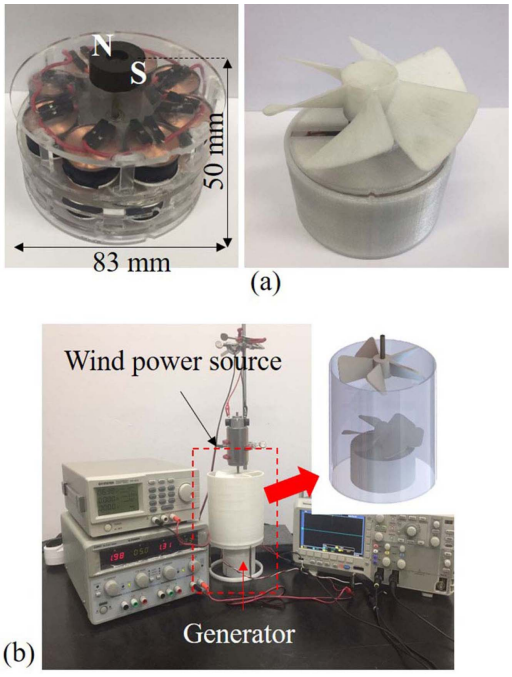

Fig. 3. (Color online) (a) The fabricated energy-harvesting devices. (b) Configuration of the experimental setup for wind input power.

(right). Apart from the propellers, the height and diameter of the device are 50 mm and 83 mm, respectively. The device housing was fabricated using 3D printer. The eight pick-up coils consist of one array and are located above and below the drive magnets. The structure is a magnetic axial coupling for magnetic induction. The air-gap between the driving magnet and the pick-up coil is 8 mm. The fabricated propeller using wind input power has six blades and diameter is 9.5 cm. Figure 3(b) show the experimental setup using wind input power.

3. Experimental Analysis

To verify the performance of the fabricated device, we conducted various experimental analyses. To measure magnetic flux density, wind velocity, and water flow with pressure, we utilized a gauss meter (F.W. Bell 5180), flow anemometer (Smart sensor AR-856), and Keyence FD-M5AY with Krone Digital Manometer KDM30, respectively. Figure 3(b) shows the experimental setup for a performance evaluation using wind input power. We installed an additional propeller at the DC motor to generate wind input power according to changes in rotating speed, and we observed air velocity with air volume using a flow anemometer to calculate the wind input power. In this paper, we mainly analyze the experimental results by wind power generation. Figure 4 shows the basic properties of the component for the device: magnetic axial coupling force, the driving range by the coupling force, and the average flux density from the inducing magnet. First, we investigated the magnetic axial-coupling force and the starting torque of the DC motor according to changes in the distance between the two coupling magnets (M1 and M2), as shown in Fig. 4(a). The starting torque at which the M2 magnet begins to rotate is determined by the coupling force (distance) between M1 and M2 magnets. A closer coupling distance leads to a larger coupling force and a higher starting torque. We observed the coupling force up to 15 mm, while distances of 3, 9, and 15 mm produced 2.634, 0.6, and 0.238 N, respectively. At the same distances, the starting torques value of the DC motor were 0.014, 0.0116, and 0.0105 Nm, respectively. Figure 4(b) shows the maximum rotating speed of the device according to the coupling distance. The device guaranteed up to 11,000 rpm at distance of 10 mm. When the distance exceeded 10 mm, the rotation speed of the disk was decreased because of the decreased coupling force with the driving torque. The maximum distance of 15 mm led to a coupling force of 0.238 N and rotation speed up to 5,712 rpm.

Figure 4(c) shows average magnetic flux density of up

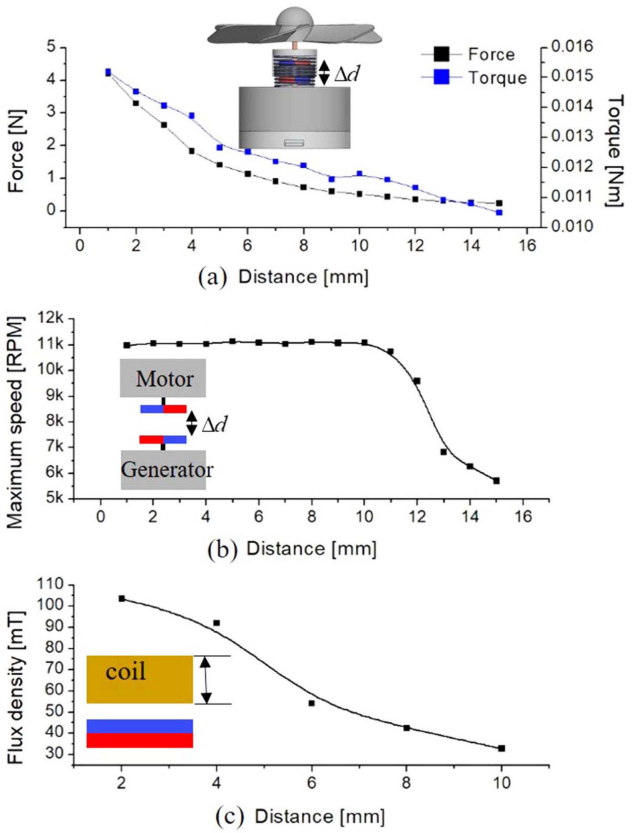

Fig. 4. (Color online) (a) Magnetic axial coupling force and the starting torque according to changes in the distance of coupling magnets between the propeller magnet and the coupling magnet on the device. (b) Maximum rotation speed according to changes in the coupling distance between the two magnets. (c) Average magnetic flux density of the driving magnet according to changes in the vertical direction (from the driving magnet to the pick-up coil).

to 10 mm from the inducing magnet. The magnetic flux density induces in the pick-up coils, while rotating speed of the inducing magnet and the magnetic flux density determines the generated voltage. The generated voltage of a rotary-type generator is proportional to the rotating speed. The rotating speeds of 60 rpm (1 Hz) and 120 rpm (5 Hz) generated 27.8 $V_{p\text{-}p}$ and 147.9 $V_{p\text{-}p}$ at no-load, respectively, as shown in Fig. 5.

It is operated up to 300 rpm to verify the performance in the low-speed rotation section. To obtain input power, we investigated air volume and wind velocity. The wind input power can be expressed as follows:

$$P_{wind} = \frac{1}{2}\rho Q v^2 \tag{5}$$

where ρ, $\boldsymbol{Q}$, and $\boldsymbol{v}$ denote the density, air volume, and wind velocity, respectively. Figure 6(a) and (b) show the

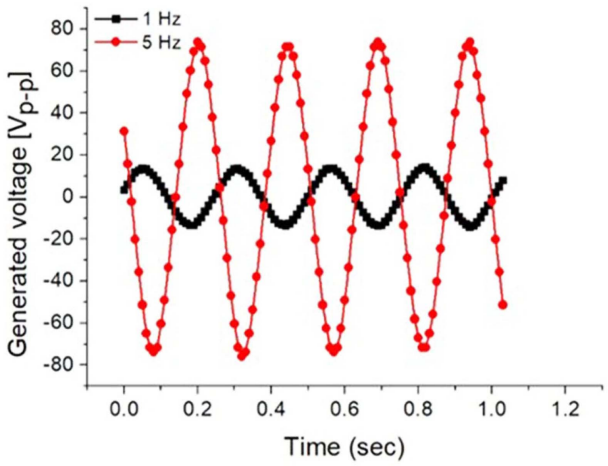

Fig. 5. (Color online) Measurement results of no-load voltage at 1 Hz (60 rpm) and 5 Hz (300 rpm) of a magnet-mounted disk.

relationship between air volume with wind velocity and the rotating speed of the magnet mounted disk. For the rotational speed of the disk to be 300 rpm, the air volume and wind velocity must differ depending on the load resistance. At lower load resistances, the electromotive force of the induction is so large that more wind speed and air volume are required than a relatively large load to reach 300 rpm. To reach 300 rpm, an air volume of 0.056 m^3/s and wind velocity of 2.77 m/s are required at 10 kΩ, whereas a load resistor of 100 kΩ requires an air volume of 0.041 m^3/s and a wind velocity of 2.07 m/s. For these reasons, the wind input power of 0.027 mW is required to generate a rotational speed of 60 rpm at a load of 10 kΩ, whereas a load of 100 kΩ requires 0.106 mW to reach 300 rpm, as shown in Fig. 6(c). Figure 6(d) shows the measurement results of the generated voltage (RMS) according to changes in the load resistances with the rotating speeds, where 60 rpm and 300 rpm generated 7.26 and 35.15 V_{rms}, respectively. Because the rotational speed is 5 times different, the generated voltage is also about 5 times different. Figure 6(e) shows the variations in the converted electrical powers. The rotating speed of 300 rpm produced a maximum power of 14.16 mW at 62 kΩ. To generate more than 1mW, the rotating speeds of 120, 180, 240, and 300 rpm require load resistances of 8.2, 3, 2, and 1 kΩ, respectively. The developed device showed a maximum conversion efficiency of 13.52 % at 240 rpm and 100 kΩ, as shown in Fig. 6(f).

4. Discussion and Conclusion

In this study, we proposed the portable rotary-type electromagnetic energy-harvesting device. In particular, the developed device adopted a detachable propeller using magnetic axial coupling, which involved removing a mechanical shaft to connect the propeller. Magnetic

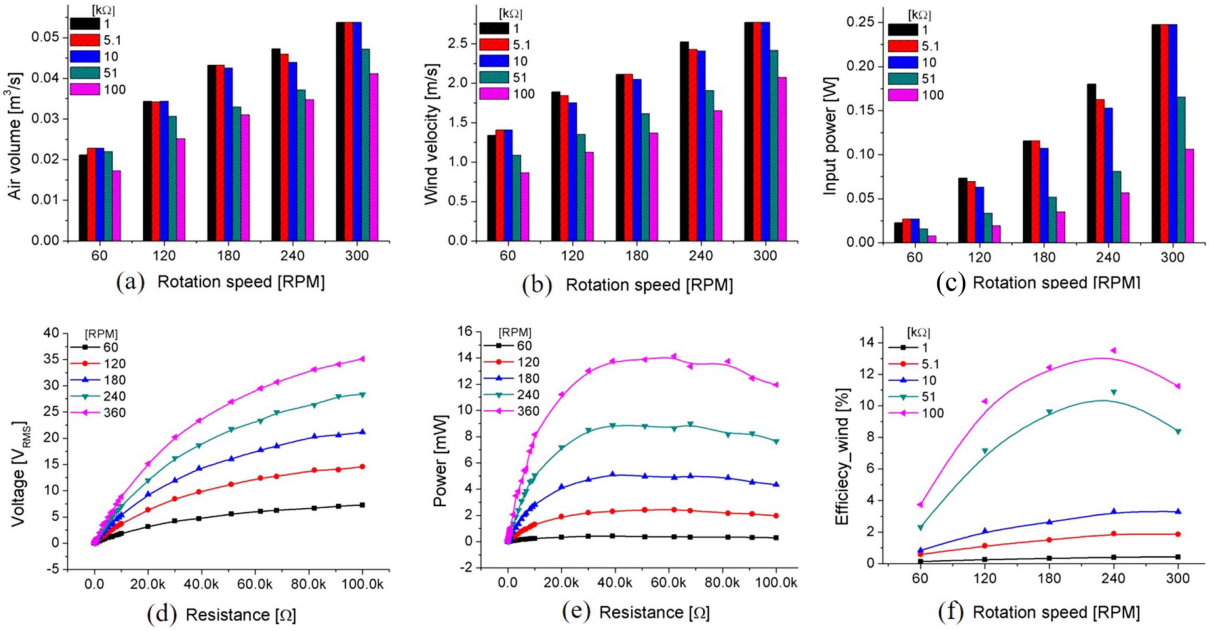

Fig. 6. (Color online) (a) The results of air volume according to changes in the rotation speed of the disk. (b) The results of wind velocity. (c) The calculated wind input power using the measured results of both the air volume and the wind velocity. (d) The measured results of the generated voltage (RMS). (e) The generated output powers (electrical power). (f) Conversion efficiency using wind input power.

force and magnetic torque from magnetic axial coupling replaced the role of mechanical shaft. The fabricated generator and the turbine are combined by the bolt-nut mechanism. Therefore, the magnetic coupling force and torque are controlled by the position of the thread of the bolt-nut mechanism. In other words, the starting torque can be adjusted by the coupling distance according to the input power. Therefore, the developed device can be applied to various applications and environments, because we can easily change the propeller depending on the input source. Generally, most generators are driven at a high-speed rotation (over thousands rrpm), whereas we achieved mW-calss energy conversion at low-speed rotation. A rotation speed of 120 rpm generated the outputs more than 1 mW and 360 rpm produced approximately 14 mW. We will consider further small sizes and solutions for a lower input power and high performance.

Acknowledgments

This research was supported by Wonkwang University in 2017.

References

[1] A. Harb, Renewable Energy **36**, 2641 (2011).
[2] H. A. Sodano, G. park, and D.J. Inman, Strain **40**, 49 (2004).
[3] F. Kahameneifar, S. Arzanpour, and M. Moallen, IEEE/ASME Trans. Mechatronics **18**, 1527 (2013).
[4] A. A. Wickenheiser, T. Reissman, W. Wu, and E. Garcia, IEEE/ASME Trans. Mechatronic*s* **15**, 400 (2010).
[5] M. Mizuno and D. G. Chetwynd, J. Micromech. Microeng. **13**, 209 (2003).
[6] C. Mo, L. J. Radziemski, and W. W. Clark, Smart Mater. Struct. **19**, 075101 (2010).
[7] M. J. Ramsay and W. W. Clark, in Proc. SPIE **4332**, 429 (2001).
[8] J. W. Sohn, S. B. Choi, and D. Y. Lee, in Proc. IMechE C. **219**, 429 (2005).
[9] F. Peano and T. Tambosso, J. Microelectromech. Syst. **14**, 429 (2005).
[10] R. Tashiro, N. Kabei, K. Katayama, F. Tsuboi, and K. Tsuchiya, J. Artifi. Organs **5**, 239 (2002).
[11] S. H. Kim, C. H. Yu, and K. Ishiyama, IEEE/ASME Trans. Mechatronics **21**, 122 (2016).
[12] D. A. Wang, C. Y. Chiu, and H. T. Pham, Mechatronics **22**, 746 (2012).
[13] R. Tashiro, N. Kabei, K. Katayama, F. Tsuboi, and K. Tsuchiya, J. Artifi. Organs **5**, 239 (2002).
[14] A. Pfenniger, L. N. Wickramarathna, R. Vogel, and V. M. Koch, Med. Eng. Phys. **35**, 1256 (2013).
[15] A. Pfenniger, R. Vogel, V. M. Koch, and M. Jonsson, Artificial Organs **38**, 68 (2014).
[16] A. P. Chandrakasan, N. Verma, and D. C. Daly, Annu. Rev. Biomed. Eng. **10**, 274 (2008).
[17] S. H. Kim, J. W. Shin, and K. Ishiyama, IEEE Trans. Magn. **40**, 4003404 (2014).